Dosimetric verification of a 3-D electron pencil beam dose calculation algorithm[a)]

D. L. McShan,[b)] B. A. Fraass, and R. K. Ten Haken
Department of Radiation Oncology, University of Michigan Medical Center, Ann Arbor, Michigan 48109

(Received 28 September 1992; accepted for publication 3 September 1993)

A three-dimensional electron beam dose calculational algorithm implemented for use in a three-dimensional treatment planning system is described. The 3-D electron beam calculations have been in use clinically for more than seven years. The algorithm uses a pencil beam model based on small angle multiple Coulomb scattering theory. Our implementation allows volumetric CT-based inhomogeneity corrections and provides for irregular field shapes (fields shaped with cerrobend cutouts) and the use of bolus. As part of NCI-funded work evaluating the state of the art in electron beam treatment planning, extensive algorithm verification was undertaken and results of these tests for our implementation are presented.

Key words: 3-D treatment planning, electron beams, pencil beams, dosimetric verification

INTRODUCTION

The use of electron beams for radiotherapy treatments is a common treatment modality for those situations where deep penetration of radiation is not needed or is undesirable.[1] In general, because of the limited range of electrons, treatment planning for electrons has largely been a matter of defining the appropriate depth of the treatment volume in order to make a selection of electron beam energy. Determination of needs for bolus, and defining the area or shape of the region to be treated are also important planning issues. In most clinics, most of these treatment planning activities are accomplished in a manual fashion (although some clinics use computerized treatment planning to assist in the selection of the appropriate electron beam energy).

The accelerators used to produce clinical electron beams commonly have a selection of electron energies. Broad uniform beams of electrons are created with a system of scattering foils and applicators (see, e.g., Refs. 2 and 3), while some machines use a scanning beam technique.[4] These electron fields are further shaped by the addition of trimmers, applicators, or blocks placed at the exit port of the beam or close to the patient. Bolus is sometimes used to reduce the depth of penetration across the radiation field. Planning treatments with these beams is complicated by the effects of electron scatter through inhomogeneous matter, by the three-dimensional variations in the shape of target volumes and surrounding anatomy, and by dose contributions from other radiation beams (electrons and photons). In order to fully plan for electron beam treatments, therefore, it is necessary to accurately predict radiation dose three dimensionally and to visualize and evaluate the distribution throughout the irradiated volume. This paper discusses the implementation and verification of a 3-D pencil beam dose calculation algorithm into the 3-D planning system developed in our department. Discussion of basic aspects of the planning system relevant to the work reported here is included in several previously published articles.[5–9]

The electron beam calculational model reported here is based on the pencil beam formalism developed by Hogstrom.[10] Our implementation includes a full three-dimensional integration of pencil beams with the ability to use irregular shaped fields. This algorithm, along with initial verification checks, was originally reported in 1985.[11] It has been used for clinical treatment planning in our department since early 1986. The calculation verification results presented here are based on the comprehensive electron beam data set[12] measured by the members of the recently completed NCI-funded contract on high-energy electron treatment planning (NCI Contract N01-67913,67914,67915, Evaluation of High Energy Electron External Beam Treatment Planning) (the Electron Contract Working Group, or "ECWG"). Although there are many reports of algorithm verification comparisons with experimental data for electron calculations,[13–16] this data set contains a more complete set of clinically relevant experiments, as well as more specific data directed toward the three-dimensional features of the dose distributions than has been reported in the past. There has been a great deal of work on 2-D implementations of the pencil beam formalism,[8,10,17–20] and that work in general is not discussed in great detail here.

In the following Materials and Method section, the calculational model and its implementation are described. The measurement techniques used for acquisition of the verification data are summarized briefly, since this work has been reported in detail elsewhere.[12] The results section presents comparisons between the 3-D calculations and the measurements. Finally, we present a discussion of the impact of accurate 3-D electron calculations for routine clinical treatment planning.

MATERIALS AND METHODS

The treatment planning system developed at the University of Michigan[5–9] has been used for all of the work described here. The system runs in a VAX/VMS operating environment on DEC VAX computers, and clinical treat-

 0094-2405/94/21(1)/13/11/$1.20

ment planning is currently based on a VAXCluster containing VAX 8820, 8700, and multiple VAXstation 4000/90 workstations. The 3-D treatment planning system, including the 3-D pencil beam algorithm discussed here, has been used for all treatment planning in the department since early 1986. The pencil beam algorithms discussed here are two of a number of calculation algorithms supported by the planning system. The complete three-dimensional anatomical,[5,8] beam,[7,9] and dose distribution descriptions[5] which are used throughout the planning system are available to the electron calculation algorithm. The system contains an extensive set of tools for entering, modifying, and displaying three-dimensional descriptions of the target volume and surrounding anatomy.[8] This information is used for three-dimensional design and evaluation of external beams[21] and brachytherapy[22] treatment plans. Volumetric dose calculations, routine use of beam's eye views and computer-designed blocks,[9,23] and use of dose volume histograms for plan evaluation[24] are included and used for routine clinical treatment planning.[25]

ECWG algorithm verification data

One of the major tasks of the NCI Electron Collaborative Working Group (ECWG) was to determine the differences in existing electron calculation algorithms and to assess the effects of these differences for clinical planning. A comprehensive set of algorithm verification test cases was agreed upon by the ECWG, and has been reported separately.[12] This data set was designed to be used for comparison of the various algorithms in a number of situations illustrating both standard measurement geometries and more complicated geometries which are important in clinical electron treatment planning. Although not designed to cover every possible circumstance, this data set does address most of the normally used clinical geometries for electron beam treatment. All test cases are based on two electron energies (9 and 20 MeV) obtained from the Varian Clinac 1800 linear accelerators at two different institutions. Field sizes of 15×15 cm (routinely used large field) and 6×6 cm (small field) were used whenever possible.

The specific data measured for each test case were determined by the ECWG. The amount of data required was made as concise as possible while maintaining enough to perform the necessary comparisons. The following general guidelines for measurements were used for each test case: (1) one or more depth dose curves (typically on central axis, measured with diode detectors in a water phantom); (2) five or more profiles for each transverse plane (often both radial and axial transverse planes were obtained, measured with the diode detector in the water phantom, and at depths chosen from the shape of the appropriate depth dose curve); (3) beam's eye view (BEV) plane (plane perpendicular to the beam central axis) dose measurements. Film in solid water phantoms was used for measurements in BEV planes, typically at depths of 2 mm and at the depth of the 90% dose line (R_{90}). The list of measurements required was modified individually for each of the 28 experimental geometries tested. The tests were divided into several groups:

(1) Basic standard geometry tests at standard and extended SSDs for two field sizes. These data are typically used for comparison and fitting of model parameters to fit the basic open field data from an individual machine. (Experiments 1–8).

(2) Field shaping tests. Using as a basis the 15×15 applicator, a simple 3×12 rectangular shaped opening, and a "house-shaped" opening were studied. In addition, two special field shaping cases were studied: (a) a craniospinal simulation involving a 5×30 opening created diagonally across the 25×25 field, and irradiated at 110 SSD, and (b) a 5-cm diameter opening in the 6×6 applicator, with a 1-cm diameter lens block in the center of the field. (Experiments 9–14).

(3) Nonperpendicular entrance tests. A beam entering the phantom at an angle of 30 degrees is used to study oblique entrance (where pencil beam algorithms often have some difficulty). A 2-D step phantom (2-cm step) was also studied. Also, an extended triangular-shaped "nose" phantom was used to investigate the 3-D effects of sharp surface irregularities. (Experiments 15–20).

(4) Heterogeneous tests. 1-D (slab), 2-D (rectangular), and 3-D (L-shaped) inhomogeneities made of air and bone substitute material were measured to characterize the behavior of the algorithms for the heterogeneity-corrected situation. (Experiments 21–28).

All data obtained for the algorithm verification dataset were obtained in one of two ways: (1) diode detectors used in a water phantom under computer control, and (2) using localization film in solid water phantoms. Depth dose, profile, and isodose chart data were collected using a diode detector as described elsewhere.[12,26] Localization film was sandwiched in a solid water film cassette and phantom material, and irradiated with approximately 6 cGy. A RFA-7 film densitometer system was used to scan all the films with a 2-mm grid of points, and the appropriate H and D curve conversions from optical density to dose were made by the RFA-7. All measured diode and film data were written to magnetic tape and exchanged among the working group members. The accuracy of the experimental measurements has been discussed in detail.[12]

We performed further analysis of the data in order to use it for quantitative comparisons against the calculated dose distributions. For each experiment, the measured profiles, depth doses, and 2-D dose grids were melded into a self-consistent (as described below) measured dose distribution for that experiment using DOSEDATA,[27] a program which is part of the planning system U-MPlan. Necessary features of this software included:

(1) Interpolation of a 2-D dose distribution from a series of profile curves and a depth dose curve. For transverse planes, the interpolation was performed along divergent ray lines. The program automatically identifies the orientation of the plane (in which the data were obtained) with respect to the phantom and beam geometries.

(2) The program automatically identifies the plane of

measurement for the film measurements. The film data must be carefully aligned with the beam used for the calculational test, since the film is often not perfectly aligned with the coordinate system of the beam. Rotation and translation of the measured doses were used to assure that the beam description and data are aligned.

(3) Some or all of the data were renormalized in order to create a self-consistent set of doses from the individual 2-D dose grids. Specifically, the various depth dose, profile, and 2-D film dosimetry dose distributions were renormalized so that the dose distributions on the multiple orthogonal planes for each experiment all were consistent at those common points or lines where the planes met. The central transverse plane dose distribution was used as the standard and, most often, the film data needed some small amounts of renormalization. Many of the blocked, inhomogeneity, and irregular surface experiments proved very difficult to make self-consistent.

(4) The program was then used to determine isodose lines in the measured dose distributions, and to take these isodose lines and add them as structures into the anatomical (phantom) distribution of the experiment. This allows the measured and calculated isodose lines to be overlaid on treatment planning system displays and hard copy plots. The measured dose lines (stored as internal structure contours in the anatomical description file) are also used as the backdrop for dose and dose difference displays, and are typically shown as dashed lines on most of the figures in this article.

Comparisons between data and calculations

Comparisons between measured and calculated dose distributions were performed using the U-MPlan Composite Plan mode.[21,27] With the composite plan program, one can take the difference between any two dose distributions ("plans") for the same case. For example, one can subtract the measured dose distribution (created in the program DOSEDATA) from the calculated dose distribution. Differences in calculation grids and limits are automatically handled by the program. Dose–volume and dose–area histograms can be generated on these dose difference composite plans if desired, and all the usual planning system dose evaluation tools can be applied. As is seen in the results section, we found that the isodose line comparison and dose difference display (overlaid on the measured isodose curves for reference) were the only analysis tools which appeared to be warranted. Although more sophisticated tools are possible, the limitations in the accuracy of both (1) the dose calculations and (2) our ability to generate accurate and self-consistent measured data sets make the sophisticated new tools unnecessary for the present.

THREE-DIMENSIONAL PENCIL BEAM MODEL

A variety of electron beam models have been developed over the last several years by various researchers (see reviews in Refs. 17, 28, and 29); including simple scaling of measured depth dose data,[30] semiempirical broad beam models,[31,32] pencil beam integration models,[18,20,33] and Monte Carlo calculations.[34,35] Probably the most commonly used and available sophisticated calculational model has been the pencil beam integration model. This type of calculation is based on small angle multiple Coulomb scattering theory. The technique generates a broad radiation field through a summation of individual pencil beams over the area of the field. With this technique, it is possible to include the effects of differential absorption and scatter in inhomogeneous media as well as irregular field shapes in the dose calculation.

Early implementations of this model[10,18–20,36] reduced the problem to a two-dimensional calculational situation in which the variations in tissue density out of the plane of calculation are assumed to be the same as that in the plane of calculation. While this assumption is not unreasonable, in most cases, the reduction to 2-D calculations has generally constrained these implementations to a limited set of calculational plane orientations. This limitation clearly limits the algorithm's usefulness in full three-dimensional dose/volume evaluations. The implementation reported here provides a fully three-dimensional pencil beam integration algorithm. The result of the 3-D calculation is a three-dimensional dose grid from which 2-D cross-sectional dose distributions can be obtained.

The formalism used here was first published by Hogstrom in 1981,[10] and is summarized with the following equation:

$$\mathrm{DOSE}(x,y,z)=\mathrm{PHOTO}(z)\times\mathrm{FOFFAXIS}(r,z)+\iint \mathrm{WGHT}(x,y,z)\times\mathrm{SCATX}(x,z)\times\mathrm{SCAT}(y,z)\,dx\,dy,$$

where x is the beam width direction, y is the beam length direction, z is the direction of central axis, r is the radial distance from central axis, PHOTO is the central axis photon depth dose, FOFFAXIS is the off-axis correction to photon dose, WGHT is the weighting factor, SCATX is the scatter contributions in x direction, and SCATY is the scatter contributions in y direction.

The weighting factor is used to normalize the dose to the measured central axis depth dose and is calculated as

$$\mathrm{WGHT}(X,Y,Z)=Do(Z_{\mathrm{eff}})\times\left(ssd+Z_{\mathrm{eff}}\right)/(\mathrm{ssd}+\mathrm{Z})\times\iint \mathrm{SAIR}(x-x',y-y',z)\,dx'\,dy'/\mathrm{SAIRXY}(z),$$

where $Do(Z_{\mathrm{eff}})$ is the measured central axis electron dose (at infinite SSD), Z_{eff} is the effective depth, SAIRXY is the air weighting factor for measured Do, SAIR is the in air weighting factor (integration over collimator aperture). The model integrates Gaussian-shaped scatter functions over the cross-sectional area of the field to get the terms SCATX, SCATY, and SAIR. The spread (or "sigma") of the Gaussian is an integral function of the linear angular scattering power, which is a product of the mass density and the mass angular scattering power[37] using the mean

electron energy (at depth). Computerized tomography (CT) density values are converted to linear stopping power ratios and to electron linear scattering power ratios. In order to account for these effects at depth, the calculations are carried out along fan lines which start at the end of the electron collimation system and progress to the maximum depth of the calculation grid. Accumulated multiple Coulomb scattering sigmas at depth are generated using a recursive technique (as described by Hogstrom[10]). In our implementation of the model, the photon contamination term PHOTO uses measured central axis depth dose data for the central ray with a radial dependence which falls linearly to zero at a fixed distance outside of the field edge.[32]

This work makes no attempt to address a number of effects which physically produce changes in the dose distribution.[28] The model does not account for the energy lost by scattered electrons. The energy loss predictions of the algorithm are an average based on water equivalent media, while in reality many of the electrons have taken different paths through the tissue, thereby losing different amounts of energy. The most observable result of this difference is in the beam penumbra where, in general, the predictable "blooming" or spreading out of the dose due to scattered electrons is calculated to occur deeper (assuming more energy) than is observed in the measurements. (Note that the electron applicators also cause perturbations to this region.) This deficiency also is expected to affect the calculational accuracy in lateral discontinuities, for example, in sinus regions. Furthermore, the model does not account for backscattered electrons and only propagates the electrons in the forward direction. Some of these problems have been addressed by other authors using an energy redefinition approach where multiple energy bins have been used to track energy fluence.[38,39]

Computer program implementation

The 3-D beam calculational code has been written in FORTRAN and was modeled after the 2-D version of the code developed at M. D. Anderson Hospital by Kenneth Hogstrom. Both a 2-D version and the new 3-D version have been integrated into our clinical treatment planning system. For both versions, speed improvements have been made by replacing time consuming interpolation, exponential, and error function calculations with "nearest neighbor" array lookups. For example, the error function is precalculated into a 5000 element array using a scaled index which takes the calculation out to a distance of 10 sigmas. To obtain an error function value, the argument of the function is used to compute an index into the precalculated array of error function values. No linear interpolation is needed due to the small step size used to initially generate the array. Typical execution times for the 3-D calculational model which is reported here are shown in Table I. In practice, these times have been found to be acceptable for routine clinical treatment planning. The ability to do quick and reasonably accurate 2-D calculations for initial planning, followed by the slower but more accurate 3-D calculations for full dose volume analysis, appears to be acceptable for most planning. As discussed later in this paper, there are, however, some situations where specific clinical problems require 3-D calculations to make even initial planning estimates.

TABLE I. Practical considerations.

Programming in FORTRAN	
Runs on a DEC VAX 32-bit supermini under VMS operating system	
Calculation speeds for 3-D Calculation, 10×10 field, 67×84×67 grid (377,076 points)	
Computer CPU	Time (min)
VAXstation 4000/90	0.96
VAX 8820	3.5
Requires large quantities of disk storage for	
Original CT scans (0.5 megabytes×128 maximum)	
Reduced density grid (8 megabytes maximum)	
Abstracted contour and surface data	
Region of interest grid (8 megabytes maximum)	
3-D calculation grids (8 megabytes maximum for each beam)	

Table II lists data and parameters which are required as fixed parameters for the calculational code. These parameters are similar to those used by Hogstrom,[10] although some parameters are determined in a different fashion than that he prescribed. Conceptually, the pencil beam formalism has been used as a parameterization of the physics, rather than as a description of the actual physical situation. One difference with the Hogstrom implementation is that the multiple scattering correction factor FMCS in the present work is modeled as linearly varying as a function of depth. The FMCS correction is obtained by linear interpolation between a value at the surface (FMCS) and one at the practical range (FMCSRP). The typical values of FMCS are about 1.4, while the FMCSRP values are less, typically 0.8 to 1.0 (for the beams described here). The 2-D and 3-D versions of the algorithm are based on the same model and do not require separate parameter sets.

The data requirements for this calculational code are the same as for our standard 3-D CT-based photon calculational code. Multiple sets of image data can be used for anatomical information, including CT, MR, PET, and SPECT.[40] For dose calculations, the user must pick a particular dataset from which the calculational geometry and

TABLE II. Input model parameters. The following data and parameters are required as fixed parameters for the calculational code.

Parameter	Function
FDD	Measured central-axis depth dose as a function of energy and field size
SCD	Source to collimator distance
SIGMA-IN	Gaussian spread of pencil in air
FMCS	Fermi multiple Coulomb scattering correction (at surface)
FMCSRP	FMCS at depth of Rp
ENERGY	Incident electron energy
SIGMA-WAT	Gaussian spread of pencil in tissue
Ao/Alambda	Collimator edge corrections

TABLE III. Calculational procedure. The following procedural steps are used in the 3-D calculational code.

Get treatment plan setup
Determine treatment volume limits
For each beam:
—Read in fixed beam data and model parameters.
—Compute fan beam grid size. The grid sizing is adjusted to cover the geometrical limits of the defined patient geometry. A maximum grid size of $101\times101\times64$ is allowed.
—Look up CT values for fan beam grid. The CT value look up uses the reduced density grid which is pregenerated on a grid interpolated from $128\times128\times N$ slices.
—Set up cross-beam block weighting factors. The field or applicator size and beam block definitions are used to generate a weighting factor grid which, presently, corresponds to the fan beam geometry grid. (This is undesirable for fan beam grids approaching 0.5 cm as the beam edge definition is undersampled.)
—Compute dose on fan beam grid. The calculation loops over the cross-beam grid points for successive depths starting (effectively) at the collimator. At each depth and grid point the in-air spread function is integrated as well as the multiple Coulomb scatter function.
—Convert to rectilinear volumetric grid. The calculational results for each of the beams is converted to a rectilinear grid which is fixed relative to a fixed reference system.
—Save dose grid. The saved dose grid for each beam is saved into a separate file.
Sum all the beams (photons and electrons) into the total dose grid and store the 3-D file.
Generate 2-D cut dose grids from 3-D grid. The 3-D grid is used to generate 2-D calculations for the prespecified cuts. In the dose evaluation procedure, new cuts can be defined and similarly generated from a summed 3-D grid.

density information is to be derived. A set of serial CT slices is normally used for 3-D planning, although manual contour entry with uniform bulk densities can be substituted. CT density data for each cut are used to generate a reduced density grid with a maximum grid size of 128×128 and a minimum grid spacing of 1 mm. The limits of the grid are sized to match the external surface limits. For most cases the grid size is about 3–4 mm. For calculations based on assigned bulk density values rather than CT data, for each cut the assigned densities (by structure) are used to fill a 512×512 array. Each structure has an assigned priority and density (in relative electron density units). The program fills the array starting with the lowest priority structures first. In case of overlap of two inhomogeneities, the user must assign a higher priority to the structure whose density is to be used for the overlap area.

For each cut of original CT (or bulk) density information, a high resolution density grid is generated by first "cleaning" the density values outside of the patient's external contour. This is done at the original image resolution, typically 512×512. Rather than using the external skin contour directly, this is accomplished by slicing the 3-D external surface description at the specified CT level. The density file always matches the number of available axial CT slices. The high resolution density file is then reduced to a 128×128 grid using averaging instead of single point sampling. The same density file is used for electron and photon beam calculations. This data generated for all slices (or cuts) thus forms a volumetric density description for the region of interest. Linear interpolation is used to compute density values for points between slices. To enhance the speed of this lookup (especially when the slices are not evenly spaced), a 128 element lookup table is generated, with each real number element defined at fixed geometrical spacing and specifying a density slice index (whole number) and an interpolation factor (fraction) between that slice and the next. This lookup table is stored along with the reduced density information in the reduced density file. This file is name coded uniquely by the case name and with an extension coded by the dataset name. This file is defined as a serial set of axial slices. Because of the data word ordering, access to the data along a specified ray will be most efficient when the ray is roughly parallel to a row of the data and least efficient when the ray intersects a single word in each row. Therefore, a second image file is generated so that the data rows are oriented in the sagittal direction. The density look up routine picks the file which yields the most efficient access time.

The density information in the reduced density file reflects a geometrical mapping and does not involve conversion to true electron (or physical) density numbers. This conversion is done as part of the electron beam calculation. The data for the conversion to electron density, as well as other conversion tables for determining electron stopping and scattering powers, are stored in a conversion file. Separate tables are included for conversion of CT number to Houndsfield units (HU), of HU to relative electron density,[41] of HU to linear collision stopping power for electrons in tissue,[10] and of HU to the projected angular scattering power.[10] Prior to calculations, the conversion tables are converted to lookup tables to allow nearest-neighbor lookups for conversion between CT numbers (as stored in the reduced density file) and the other dependent data (i.e., four separate tables for HU, reduced electron densities, electron stopping power, and angular scatter power).

The procedural steps used in the 3-D calculational code are summarized in Table III. For a given beam, the calculation begins by computing the fan beam grid sizing. The fan beam grid is uniformly spaced along the central plane ($z=0$) and across the perpendicular cross-beam plane ($x=0$). The grid sizing is adjusted for depth to cover the geometrical limits of the defined patient geometry. The

cross-beam spacing is calculated to 3 cm beyond the geometrical field edges. A maximum pencil fan beam grid size of $101 \times 101 \times 64$ is allowed. In order to predict the effects of inhomogeneities, CT values for each grid element are found by interpolation from the pregenerated reduced three-dimensional density grid. (The grid volumes for the two grids are approximately the same so that the need for extra sampling is eliminated.)

The program allows calculations with density corrections turned off. In this case, the fan beam density grid is generated by filling the grid elements inside the external skin surface with a density of 1.0. This is done by slicing the external surface on diverging planes and filling the interior. This same technique is used to handle the addition of bolus, with the exception that the bolus density is not allowed to override existing density numbers (nonzero). This allows the bolus volume to be designed with only the surface closest to the radiation being significant. Use of bolus internally is, however, allowed to override other density numbers.

The next step in the procedure is to generate the cross-beam block weighting factors. The field, applicator size, and beam block definitions are used to generate a weighting factor grid which corresponds to the fan beam geometry grid. The weighting factors are sampled at twice the cross-beam grid spacing and averaged. The weighting factors are currently defined to be 1.0 within the open field definition and 0.0 outside. At present, transmission through trimmer blocks is not included. Inclusion of transmission effects could be made but will need appropriate changes in energy and scattering effects. This method of determining the pencil weights is used for both 2-D and 3-D pencil beam models, so that the only significant difference between the 2-D and 3-D implementations of the model is in how three-dimensional inhomogeities are handled by the 2-D or 3-D pencil beam integrations.

With these precalculation steps performed, the calculation then loops over the cross-beam grid points for successive depths starting (effectively) at the collimator. At each depth and grid point, the in-air spread function is integrated as well as the multiple Coulomb scatter function. Following the calculations, the results computed with the fan beam geometry are then converted to a rectilinear grid which is fixed to the patient. This dose grid is saved in separate files for each beam calculated. The 3-D grids for all beams calculated are then summed into the total dose file. Dose readouts can be in the form of individual point readouts, one-dimensional (1-D) profiles, two-dimensional (2-D) cross-sectional isodose lines, or 3-D isodose surfaces (see Ref. 21).

RESULTS

While all 28 experiments mentioned above were analyzed as part of the NCI contract work, we have selected a limited number of results, all obtained for the 20-MeV electron beam, for presentation in this article. This consistency in subject matter will allow the reader to directly relate the results of the various tests to one another, so that an overall impression of the accuracy of the algorithm is

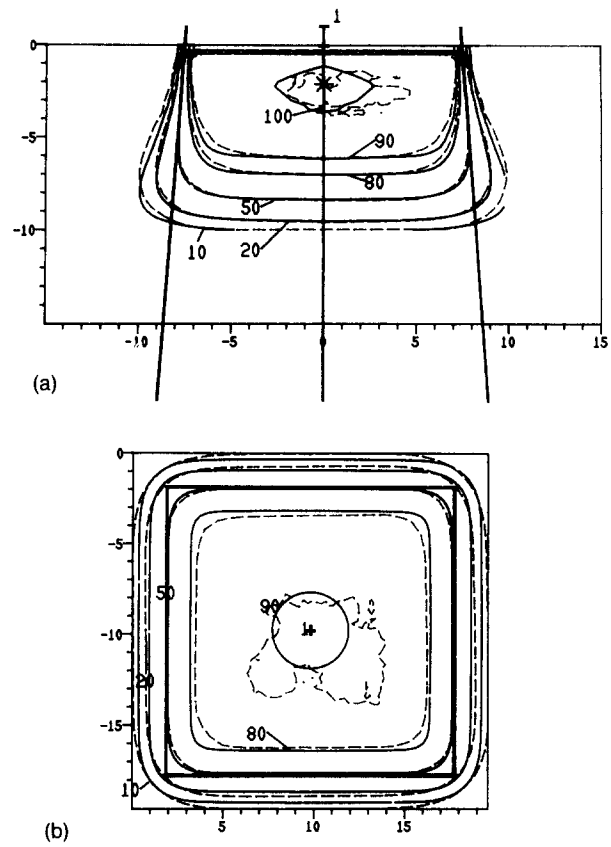

FIG. 1. ECWG experiment 3–1: open field, 20 MeV, 15×15, 100 SSD. Solid lines show results from calculations, while the dashed lines are the isodose lines obtained from the measured data. (a) Transverse central axis plane. (b) Coronal (BEV) plane at depth=6.1 cm.

formed. All dose calculations were carried out on a 2.5-mm grid, and the data measured on a grid of 2 mm or less, so there should be few grid-specific effects,[42] except for the depth dose sensitivity this grid causes, since 2 mm in depth dose is typically 5% or more on the steep part of the electron depth dose curve. All isodose plots were normalized to the measured plan normalization dose points specified in the measurement protocol.[12]

Figure 1 shows the standard 15×15 cm field at 100-cm source to surface distance (SSD). Figure 1(a) compares the 3-D calculation (solid lines) versus the measurements (dashed lines) on the transverse central axis plane. The agreement is generally good, with the largest errors near the 10% isodose line in the penumbral region, where there is a maximum error of 4% (calculated % dose-measured % dose). This particular region (where the isodose lines bow out) is an area in which the doses calculated are sensitive to the lack of correct handling of the change in energy distribution during multiple scattering, as well as effects related to the details of the design of the applicators. Although it is possible to manipulate pencil beam parameters so that the agreement for this case is better, that manipulation is done at the expense of having less good agreement as the SSD increases. We have opted to choose parameters so that the agreement at 110 SSD (see Fig. 3) is not worse than that at 100 SSD. Figure 1(b) shows the 3-D algorithm on a plane perpendicular to the central axis

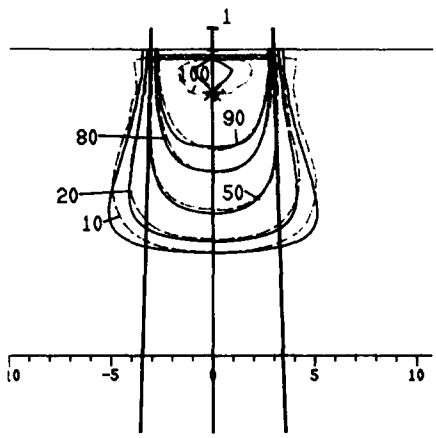

FIG. 2. ECWG experiment 4–1: open field, 20 MeV, 6×6, 100 SSD. Solid lines show results from calculations, while the dashed lines are the isodose lines obtained from the measured data on the transverse central axis plane.

(BEV plane) at a depth of 6.1 cm. Overall, the agreement is excellent except for the corners of the applicator and for the outer penumbra region [as seen in Fig. 1(a)]. The rounded corners in the Varian electron cone aperture are presently modeled with square corners, explaining the discrepancy in the applicator corners. Further open field results are shown in Figs. 2 and 3. Figure 2 shows the 20-MeV 6×6 field at 100 SSD, on the central transverse plane, with very good agreement. Any disagreements between the calculations and measurements of the central axis depth dose for square fields at the standard SSD are due to grid effects in the 3-D surface description and density grids which are used to describe the phantom setup, since the algorithm in principle should reproduce the input depth dose curves for these situations. Figure 3 illustrates the agreement which is achieved with an experiment performed at 110 SSD with the 15×15 field. The agreement between calculation and experiment is excellent, even though the depth dose at 110 SSD for this situation is different than that at 100 SSD. As described before, the values of the sigmas and effective source locations have

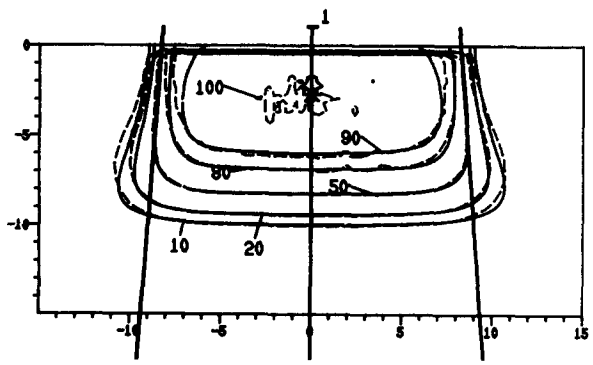

FIG. 3. ECWG experiment 7–2: open field, 20 MeV, 15×15, 110 SSD. Solid lines show results from calculations, while the dashed lines are the isodose lines obtained from the measured data shown on the transverse central axis plane.

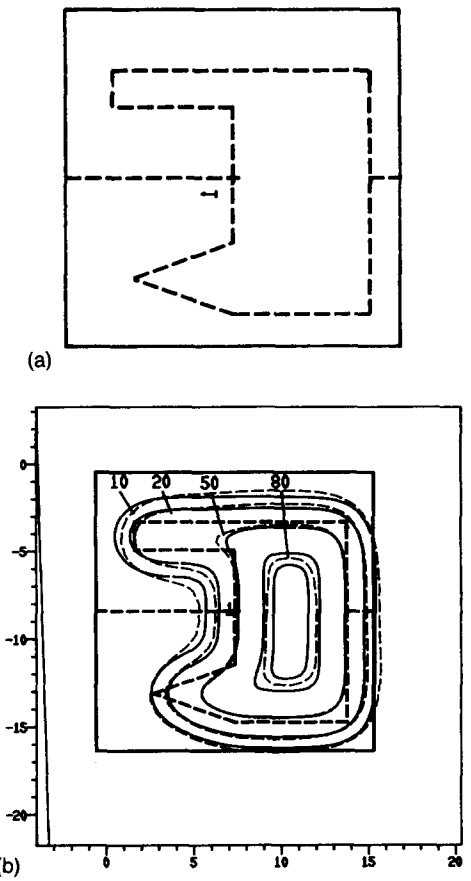

FIG. 4. ECWG experiment 12–4: "House block," 20 MeV, 15×15 field, 100 SSD. (a) A plot of the shadow of the house-shaped block is shown on this coronal cut at a depth of 0.2 cm below the surface of the phantom. (b) The calculation results (solid lines) are plotted versus the isodose lines extracted from the measured data (dashed lines) on the coronal cut at depth $d=6.1$ cm.

been set so that the model more correctly predicts the change in depth dose as the SSD changes, although all field size dependent changes are not yet handled. However, within the current model, this agreement is achieved by sacrificing some accuracy in the region near the surface of the patient (see, e.g., Fig. 3). However, this has been deemed clinically appropriate in our clinical setting.

In order to investigate irregularly shaped fields, a "house" shaped field was devised to test the algorithm under somewhat extreme situations. Figure 4(a) demonstrates the block shape used with the 15×15 field, and Fig. 4(b) shows the results of the 3-D algorithm for the coronal cut at 6.1-cm deep. There is excellent agreement between the calculation and the data.

Figure 5 shows a 15×15 field entering the phantom at an angle of 30 degrees to the perpendicular. The central axis plane illustrates the agreement between 3-D calculations and the data. The most noticeable effect is the ripple in the calculation near dmax, which is caused by the slab method used of propagating the pencil beams through the phantom. A smaller grid size minimizes these effects, but is often difficult to accomplish within the constraints of planning system limitations (our overall calculation grid is limited to 128×128×128). The magnitude of these errors is

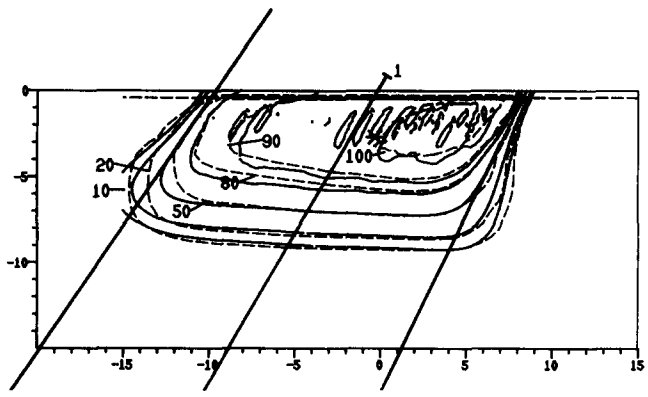

FIG. 5. ECWG experiment 16–7: Open 15×15 field, 20 MeV beam, with the beam entering the phantom at an angle of 30 degrees from perpendicular, central axis transverse slice. The calculation results are shown as solid lines, while the data are shown as dashed lines.

about ±2%. The largest discrepancy, however, is at the distal end of the field, where nearly 10% error in the dose at depth was found. Note here that the profile measurements (and the resulting measured isodose chart) on which the comparison is based were limited in this region.

A more extreme test of the algorithm's ability to deal with nonperpendicular incidence is an experimental situation resembling a nose. As shown by the external contour shape in Fig. 6(a), a sharp simulated nose was placed on top of a flat water phantom. On the central transverse plane [Fig. 6(a)], the algorithm shows excellent agreement between calculations and measurements. The 120% hot spots on either side of the nose are predicted to within about 1% accuracy, while the cold spot below the nose is within 5% (on a very high gradient part of the depth dose curve). Figure 6(b) shows results for a coronal plane at a depth of 6.1 cm for the algorithm.

To investigate inhomogeneities, a number of 1-D, 2-D, and 3-D inhomogeneity experiments were performed. Figure 7 shows the comparison of the calculations versus the measured data for a linear 1 cm×4 cm air cavity. This central axis transverse cut shows the characteristic higher dose in the shadow of the edges and slightly lower dose outside of this region. The calculation shows excellent agreement everywhere, with almost the entire area less than 2% different from the measured data.

A more complex inhomogeneity test is the use of an L-shaped bone placed approximately 1-cm deep inside the phantom. Figure 8(a) shows a coronal cut at a depth of 1.5 cm, through the middle of the bonelike inhomogeneity. Figure 8(b) shows the dose calculations on a transverse plane 1 cm from the thick part of the bone, and illustrates excellent agreement between calculations and data. As shown by the results for the coronal plane (d=6.1 cm), the 3-D algorithm predicts with very good accuracy all of the basic effects shown in the measured data, including the hot spots off the edges of each section of the bone. Although the calculations disagree with the data by several percent at this depth, one should remember that a 5% change in dose at this depth corresponds to a 2-mm change

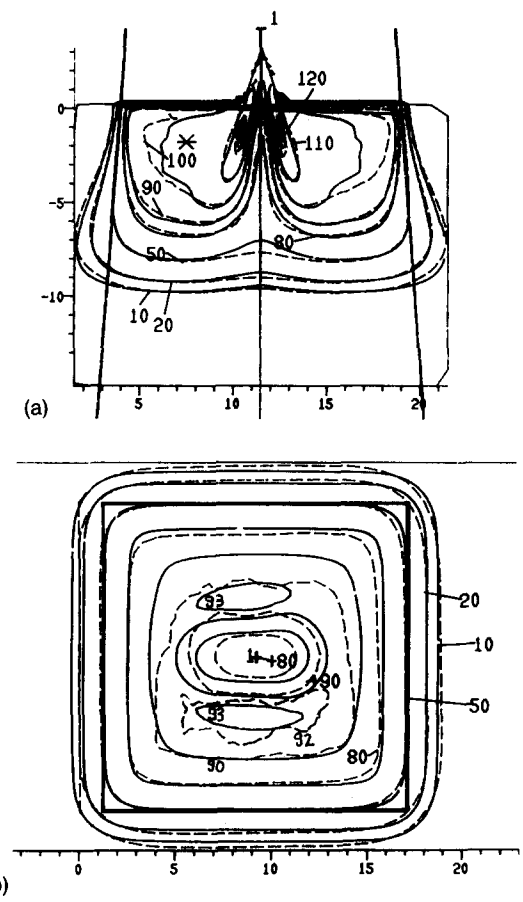

FIG. 6. ECWG experiment 20–9: Nose phantom, 15×15 field, 20 MeV, with 100 SSD to flat phantom. (a) Calculations (solid lines) are compared to measured data (dashed lines) for the central transverse cut. (b) Calculation (solid) versus measured data (dashed lines) for the coronal plane at depth 6.1 cm.

in depth (the resolution of the calculation grid was only 2.5 mm in these calculations). The hotspot values agree within 1%. The algorithm does an excellent job of predicting the change in scatter due to the 3-D shape of the inhomogeneity.

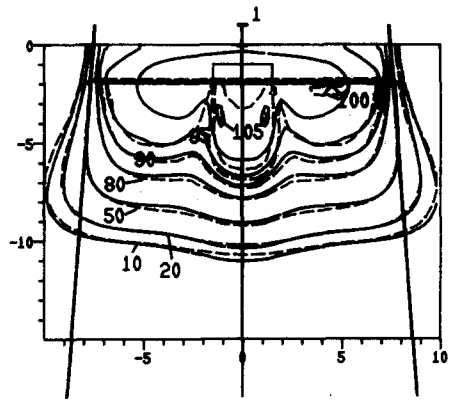

FIG. 7. ECWG experiment 26–13, a linear air cavity with 20 MeV electrons and 15×15 field size at 100 SSD. Calculations (solid) are displayed versus measured data (dashed lines) on the central axis transverse slice.

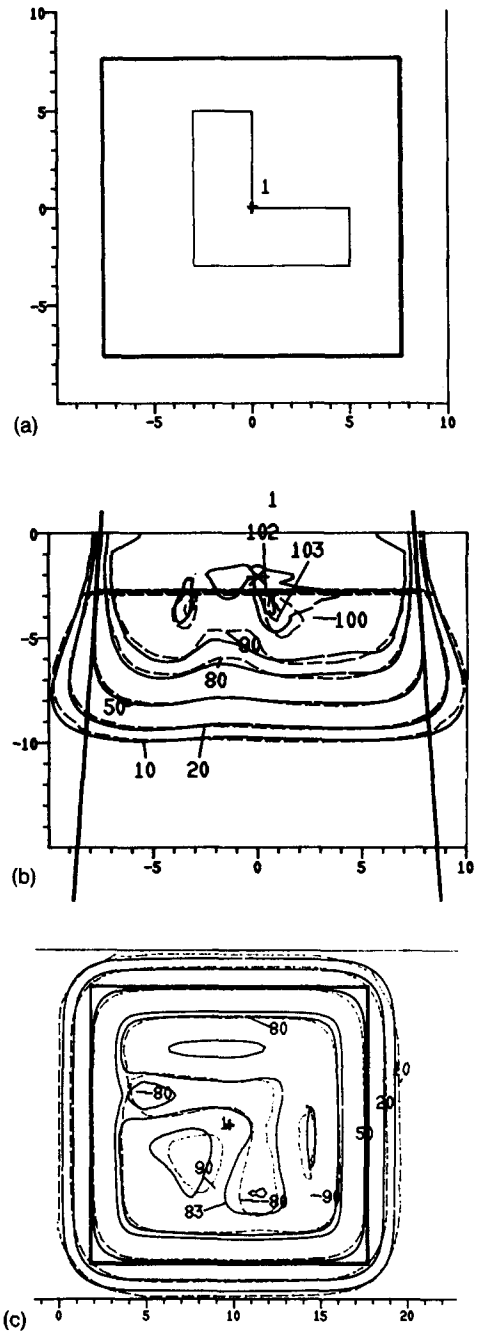

FIG. 8. ECWG experiment 28–14:L-shaped bone inhomogeneity, 20 MeV electrons, 15×15 field, 100 SSD. (a) Display of bone inhomogeneity in a coronal cut 1.5 cm below the phantom surface. (b) Calculation (solid) plotted versus the measured data (dashed lines) on a transverse cut 1 cm from the thick section of the bone inhomogeneity. (c) Calculation (solid) plotted versus the measured data (dashed lines) on a coronal cut at depth 6.1 cm.

DISCUSSION

The 3-D pencil beam algorithm described here performs very well in many situations, however, it can be significantly improved in others. The general agreement between data and calculation is very good. Most differences are in very high gradient regions (back side of depth dose, or the penumbra). These differences can typically be more than 3%, but those dose differences almost always correspond to distances less than 2 mm. Since the rectilinear calculation grid (and pencil beam spacing at the isocentric distance) were both between 2.5 and 3 mm, nearly all errors are within the grid spacings which were used. This highlights the importance of all of the grid sizes which figure into the calculations and their comparisons with measurements: these include (1) the rectilinear calculation grid (typical spacing between 2 and 5 mm), (2) the precision of the depth calculations (here, same as the grid spacing), (3) the resolution of the 3-D density grid (here, between 3 and 6 mm, dependent on patient/phantom size), (4) the size of surface tiles used to describe the 3-D patient surface (dependent on the spacing between CT slices, and then number of tiles used per surface), and (5) the pencil beam spacing (here, typically set to the same size as the rectilinear grid spacing), (6) the resolution of the measurements for the experiment, and (7) the accuracy with which the experimental setup (and the data) can be registered with the calculational experimental setup. Furthermore, the self-consistency of the data obtained on different cuts for the same experimental setup is often a larger error than the differences which have been found between calculations and data.

Two issues could be improved significantly by some relatively simple changes in the implementation of the algorithm. The first is the large differences in the doses at the corners of the BEV plots; this is caused by the fact that the model implementation presented here does not model the curved corners of the applicator inserts. A more important problem is that the present implementation does not allow for applicator-dependent parameters. In order to accurately model the dose from each applicator, applicator-dependent flatness (pencil beam weight factors), and applicator-dependent corrections for behavior at the edge of the field should be added. In a development version of the planning system, objects called electron applicators have been defined, so that for each applicator, the aperture shape, and the other pencil beam parameters, can be defined individually. These features are being tested and will be reported separately.

While the field flatness parameters are really only important for large (20×20 and 25×25) applicators, the field edge behavior is always important, particularly for electron applicator systems which utilize in-scatter from the applicator to help flatten the dose distribution. Since these applicator-dependent factors are not included in the current model, determination of the pencil beam parameters for each electron beam involves making a compromise between the behavior for the various applicator sizes. In the results described here, the calculation model parameters have been optimized using the 6×6 and 15×15 applicators for reference. Therefore, the fit of the calculations to the data for the small field experiments could be improved at the expense of the larger field behavior, or vice versa.

One more parameterization-dependent factor is apparent here (especially when compared to other pencil beam model implementations[10]). Several of the basic pencil beam model parameters have been considered as fitting parameters, rather than forcing these parameters to be exactly derived according to the usual methods (see Ref. 10, for

example). These include the virtual source distances, and the Gaussian spreads (sigmas) used in the model. By allowing these parameters to be changed, the SSD dependence of the calculated depth dose was made to agree more closely with the basic beam data. The tradeoff is that the behavior of the penumbra of the calculated dose from the surface to near dmax disagrees more with the data than is usual for a pencil beam model. Although this behavior near the surface is not as "pretty" as one might like, a clinical judgment was made that the SSD behavior was more important. Obviously, the SSD dependence of the model should be improved so that the above-described tradeoff decision is not necessary.

The 3-D electron calculation algorithm has been used clinically at the University of Michigan since March 1986. The accuracy of the calculation verification tests which are reported here, along with earlier work comparing 2-D and 3-D calculation results (not reported here) have confirmed our opinion that dose calculations for electron beam treatment planning should typically be performed with a 3-D calculation model, and should be performed throughout the 3-D volume of interest. This work has pointed out how important a small calculation grid is; we now use a 3-mm (or less) calculation grid spacing for electron calculations unless there is some other compelling reason to use a larger grid. A 2-D version of this model is sometimes used for initial plan optimization on several slices, but for clinical use, the 3-D algorithm is always used for the calculation of the final dose distribution.

A large number of pencil beam and other electron dose calculation algorithms have been reported in the literature over the years (see review in Ref. 15). Except for the recently reported 3-D pencil beam models of Shiu,[38] Yu,[39] and Kooey,[43] however, all of the other work has been generally two-dimensional in nature. Much of the recent development work has been in the area of the pencil beam redefinition models,[38,39] which attempt to improve on some of the basic algorithmic limitations of the current pencil beam model. Note that the aim of this present work was not the creation of an entirely new algorithm, but rather the practical implementation of a well-known formalism, without the 2-D approximations which are usually used, and to implement these complex calculations with enough efficiency and accuracy that the resulting dose calculations were fast enough and accurate enough to be used for routine clinical 3-D treatment planning.

CONCLUSIONS

Electron pencil beam models have been extensively used for electron beam dose calculations for a number of years. This paper describes the extension of the 2-D Hogstrom electron pencil beam model[10] to a fully three-dimensional model. Extensive algorithm verification tests have been performed, and are reported here. Dosimetric agreement between calculations and measurements is generally very good, with nearly all disagreements in location of isodose lines within the size of the grid size used for the calculations and/or the measurements. The model reported here has been used for clinical treatment planning for six years in a wide variety of clinical sites. The calculational code represents a useful tool for exploring the accuracy and limits of volumetric planning evaluations in clinical practice. Due to the necessity of using the 3-D calculational model for clinical cases, optimization of the operation of the algorithm has been of great importance, so that calculation times are short enough for routine clinical use.

ACKNOWLEDGMENTS

We would like to acknowledge the work of John Wong, Russ Gerber, and Bill Harms (Washington University, St. Louis), Almon Shiu and Ken Hogstrom (University of Texas M. D. Anderson Cancer Center), and Karen Hutchins (University of Michigan) for assistance during the ECWG algorithm verification data measurements, Robert Morton and Sandra Zink from the National Cancer Institute for their work helping to foster an excellent working relationship within the Electron Contract Working Group, and Mark LaVigne for work on the algorithm verification calculations and analysis. Supported in part by NCI Contract No. N01-CM-67913.

[a]Presented in part at the 1985 meeting of the American Association of Physicist in Medicine, Seattle, Washington, August, 1985.

[b]Reprint requests to: Daniel L. McShan, Ph. D., Department of Radiation Therapy, University of Michigan Hospitals, AGH Room B2C490, Box 0010, 1500 E. Medical Center Dr., Ann Arbor, Michigan 48109.

[1]N. du V. Tapley, *Clinical Applications of the Electron Beam* (Wiley, New York, 1976).

[2]P. R. Almond, "Characteristics of current medical electron accelerator beams," in *Proc. Symp. Electron Beam Therapy*, edited by F. Chu and J. S. Laughlin (Sloan-Kettering Cancer Center, New York, 1981), pp. 43–49.

[3]T. H. Kirby, R. J. Gastorf, W. F. Hansen, L. W. Berkley, W. F. Gagnon, J. D. Hazle, and R. J. Shalek, "Electron beam central axis depth dose measurements," Med. Phys. **12**, 357–361 (1985).

[4]A. Brahme, T. Kraepelien, and H. Svensson, "Electron and photon beams from a 50 MeV racetrack microtron," Acta Radiol. Oncol. **19**, 305–319 (1980).

[5]B. A. Fraass and D. L. McShan, 3-D Treatment planning. I. Overview of a clinical planning system," in *The Use of Computers in Radiation Therapy*, edited by I. A. D. Bruinvis, P. H. van der Giessen, H. J. van Kleffens, and F. W. Wittkamper (Elsevier Science, North-Holland, 1987), pp. 273–276.

[6]B. A. Fraass, D. L. McShan, R. K. Ten Haken, and K. M. Hutchins, "3-D treatment planning. V. A fast 3-D photon calculation model," in *The Use of Computers In Radiation Therapy*, edited by I. A. D. Bruinvis, P. H. van der Giessen, H. J. van Kleffens, and F. W. Wittkamper (Elsevier Science, North-Holland, 1987), pp. 521–524.

[7]B. A. Fraass, D. L. McShan, and K. J. Weeks, "3-D treatment planning. III. Complete beam's-eye-view planning capabilities," in *The Use of Computers In Radiation Therapy*, edited by I. A. D. Bruinvis, P. H. van der Giessen, H. J. van Kleffens, and F. W. Wittkamper (Elsevier Science, North-Holland, 1987), pp. 193–196.

[8]D. L. McShan and B. A. Fraass, "3-D treatment planning. II. Integration of gray scale images and solid surface graphics," in *The Use of Computers In Radiation Therapy*, edited by I. A. D. Bruinvis, P. H. van der Giessen, H. J. van Kleffens, and F. W. Wittkamper (Elsevier Science, North-Holland, 1987), pp. 41–44.

[9]D. L. McShan, B. A. Fraass, and A. S. Lichter, "Full integration of the beam's eye view concept in clinical treatment planning," Int. J. Rad. Oncol. Biol. Phys. **18**, 1485–1494 (1990).

[10]K. R. Hogstrom, M. D. Mills, and P. R. Almond, "Electron beam dose calculations," Phys. Med. Biol. **26**, 445–459 (1981).

[11]D. L. McShan, B. A. Fraass, R. K. Ten Haken, and R. Jost, "Three-dimensional electron beam dose calculations and dosimetric evaluations," Med. Phys. **12**, 507 (1985) [Abstract].

[12]A. S. Shiu, S. Tung, K. R. Hogstrom, J. W. Wong, R. L. Gerber, W. B. Harms, J. A. Purdy, R. K. Ten Haken, D. L. McShan, and B. A. Fraass, "Verification data for electron beam dose algorithms," Med. Phys. **19**, 623–636 (1992).

[13]J. Cygler, J. J. Battista, J. W. Scrimger, E. Mah, and J. Antolak, "Electron dose distributions in experimental phantoms: A comparison with 2D pencil beam calculations," Phys. Med. Biol. **32**, 1073–1086 (1987).

[14]K. R. Hogstrom and P. R. Almond, "Comparison of experimental and calculated dose distributions," in Acta Radiologica, Suppl. **364**, 89–102 (1983).

[15]E. Mah, J. Antolak, J. W. Scrimger, and J. J. Battista, Experimental evaluation of a 2D and 3D electron pencil beam algorithm," Phys. Med. Biol. **34**, 1179–1193 (1989).

[16]B. J. McParland, J. R. Cunningham, and M. K. Woo, The optimization of pencil beam widths for use in an electron pencil beam algorithm," Med. Phys. **15**, 489–497 (1988).

[17]A. Brahme, I. Lax, and P. Andreo, "Electron beam dose planning using discrete Gaussian beams," Acta Radiol. Oncol. **20**, 147–158 (1981).

[18]I. A. D. Bruinvis, R. van de Laarse, W. A. F. Mathol, and M. F. Nooman, "An electron beam dose planning method for arbitrary field shapes, "*Proceedings of the Eighth International Conference on the Use of Computers in Radiation Therapy* (IEEE Computer Society, Toronto, 1984), pp. 152–156.

[19]K. R. Hogstrom, M. D. Mills, J. A. Meyer, J. R. Palta, D. E. Mellenberg, R. T. Meoz, and R. S. Fields, "Dosimetric evaluation of a pencil-beam algorithm for electrons employing a two-dimensional heterogeneity correction" Int. J. Radiat. Oncol. Biol. Phys. **10**, 361–369 (1984).

[20]I. Lax, "Inhomogeneity corrections in electron beam dose planning. Limitations with the semi-infinite slab approximation," Phys. Med. Biol. **31**, 879–892 (1986).

[21]D. L. McShan, "Treatment plan evaluation and optimization," in *Syllabus: Radiation Therapy Treatment Planning*, edited by B. R. Paliwal and M. L. Griem (RSNA, Chicago, 1986), pp. 33–40.

[22]R. K. Ten Haken, R. F. Diaz, D. L. McShan, B. A. Fraass, J. A. Taren, and T. W. Hood, "Manual vs computerized planning and dosimetry for stereotactic brain implants," Int. J. Rad. Oncol. Biol. Phys. **15**, 467–480 (1988).

[23]B. A. Fraass, D. L. McShan, and K. J. Weeks, *Computerized Beam Shaping in Computers in Medical Physics*, edited by A. R. Benedetto, H. K. Huang, and D. P. Ragan (American Institute of Physics, Woodbury, NY, 1990), pp. 333–340.

[24]T. S. Lawrence, R. J. Tesser, and R. K. Ten Haken, "An application of dose volume histograms to treatment of intrahepatic malignancies with radiation therapy," Int. J. Radiat. Oncol. Biol. Phys. **19**, 1041–1047 (1990).

[25]B. A. Fraass, Clinical utility of 3-D treatment planning, "in *Advances in Radiation Oncology Physics: Dosimetry, Treatment Planning and Brachytherapy*, edited by J. A. Purdy (American Institute of Physics, Woodbury, NY, 1992), pp. 967–997.

[26]R. K. Ten Haken, B. A. Fraass, and R. J. Jost, "Practical methods of electron depth-dose measurement compared to use of the NACP design chamber in water" Med. Phys. **14**, 1060–1066 (1987).

[27]R. L. Stern, B. A. Fraass, A. Gerhardsson, D. L. McShan, and K. L. Lam, "Generation and use of measurement-based 3D dose distributions for 3D dose calculation verification," Med. Phys. **19**, 165–173 (1992).

[28]K. R. Hogstrom, G. Starkschall, and A. Shiu, "Dose calculation algorithms for electron beams," in *Advances in Radiation Oncology Physics: Dosimetry, Treatment Planning and Brachytherapy*, edited by J. A. Purdy (American Institute of Physics, Woodbury, NY, 1992), pp. 900–924.

[29]R. Mohan, R. Riley, and J. S. Laughlin, "Electron beam treatment planning: A review of dose computation methods," in *Computed Tomography in Radiation Therapy*, edited by C. C. Ling, C. C. Rogers, and R. J. Morton (Raven, New York, 1983), pp. 229–239.

[30]F. M. Khan and J. M. F. Lee, "Computer algorithm for electron beam treatment planning," Med. Phys. **6**, 142–144 (1979).

[31]J. G. Holt, R. Mohan, R. Caley, A. Buffa, A. Reid, L. Simpson, and J. S. Laughlin, Memorial electron beam AET treatment planning system, in *Practical Aspects of Electron Beam Treatment Planning*, Medical Physics Monograph No. 2, edited by C. G. Orton, and F. Bagne (American Institute of Physics, Woodbury, NY, 1978), pp. 70–79.

[32]J. van de Geijn and B. A. Fraass, "Application of the projective dose field model to clinical electron beams," *Proceedings of the Seventh International Congress of Radiation Research*, edited by J. J. Broerse (Nijhoff, Amsterdam, 1983), p. E2–15.

[33]P. R. M. Storchi and H. Huizenga, "On a numerical approach of the pencil beam model," Phys. Med. Biol. **30**, 467–473 (1985).

[34]A. F. Bielajew, D. W. O. Rogers, J. Cygler, and J. J. Battista, "A comparison of electron pencil beam and Monte Carlo calculational methods," in *The Use of Computers in Radiation Therapy*, edited by I. A. D. Bruinvis, P. H. van der Giessen, H. J. van Kleffens, and F. W. Wittkamper (Elsevier Science, North-Holland, 1987), pp. 65–68.

[35]T. R. Mackie, "Calculating electron dose using a convolution/superposition method," in *The Use of Computers in Radiation Therapy*, edited by I. A. D. Bruinvis, P. H. van der Giessen, H. J. van Kleffens, and F. W. Wittkamper (Elsevier Science, North-Holland, 1987), pp. 445–448.

[36]D. Perry and G. Holt, "A model for calculating the effect of small inhomogeneities on electron beam dose distributions," Med. Phys. **7**, 207–215 (1980).

[37]International Committee on Radiation Units (ICRU), Radiation Dosimetry: Electrons with Initial Energies Between 1 and 50 MeV, ICRU Report 21, Washington, DC (1972).

[38]A. S. Shiu and K. R. Hogstrom, "Pencil beam redefinition algorithm for electron dose distributions," Med. Phys. **18**, 7–18 (1991).

[39]C. S. Yu, W. S. Ge, and J. W. Wong, "A multiray model for calculating electron pencil beam distribution," Med. Phys. **15**, 662–671 (1988).

[40]B. A. Fraass, D. L. McShan, R. F. Diaz, R. K. Ten Haken, A. Aisen, S. Gebarski, G. Glazer, and A. S. Lichter, "Integration of MRI into radiation therapy treatment planning," Int. J. Rad. Oncol. Biol. Phys. **13**, 1897–1908 (1987).

[41]A. A. Mustafa and D. F. Jackson, Phys. Med. Biol. **28**, 169–176 (1983).

[42]A. Niemierko and M. Goitein, "The influence of the side of the grid used for dose calculations on the accuracy of the dose estimation," Med. Phys. **16**, 239–247 (1989).

[43]H. M. Kooey and H. Rashid, "A three-dimensional electron pencil beam algorithm," Phys. Med. Biol. **34**, 229–243 (1989).